JACS
JOURNAL OF THE AMERICAN CHEMICAL SOCIETY
Article
pubs.acs.org/JACS

Segregation of Sublattice Domains in Nitrogen-Doped Graphene

Amir Zabet-Khosousi,[†] Liuyan Zhao,[‡] Lucia Pálová,[†] Mark S. Hybertsen,[§] David R. Reichman,[†] Abhay N. Pasupathy,[‡] and George W. Flynn*[,†]

[†]Department of Chemistry, Columbia University, New York, New York 10027, United States
[‡]Department of Physics, Columbia University, New York, New York 10027, United States
[§]Center for Functional Nanomaterials, Brookhaven National Laboratory, Upton, New York 11973, United States

Supporting Information

ABSTRACT: Atomic-level details of dopant distributions can significantly influence the material properties. Using scanning tunneling microscopy, we investigate the distribution of substitutional dopants in nitrogen-doped graphene with regard to sublattice occupancy within the honeycomb structure. Samples prepared by chemical vapor deposition (CVD) using pyridine on copper exhibit well-segregated domains of nitrogen dopants in the same sublattice, extending beyond 100 nm. On the other hand, samples prepared by postsynthesis doping of pristine graphene exhibit a random distribution between sublattices. On the basis of theoretical calculations, we attribute the formation of sublattice domains to the preferential attachment of nitrogen to the edge sites of graphene during the CVD growth process. The breaking of sublattice symmetry in doped graphene can have important implications in its electronic applications, such as the opening of a tunable band gap in the material.

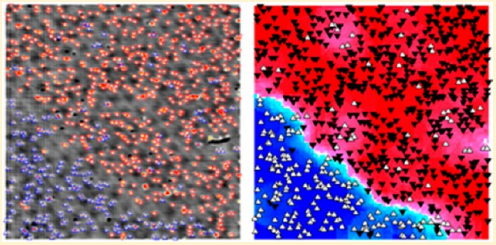

INTRODUCTION

Substitutional doping of a crystal offers a robust approach for modifying the crystal's properties, through the introduction of foreign atoms into the host lattice structure.[1,2] However, in addition to the structure and composition of individual dopants, the spatial distribution of the dopants also constitutes an important factor that can be used to control material properties.[3] For example, in nanoscale semiconductor devices, ordered versus randomly distributed dopants have been shown to significantly enhance device performance.[4] Therefore, atomic-level control over dopant distributions provides an important characteristic to be considered in the development of functional nanomaterials. With recent advances in the formation of two-dimensional materials such as graphene, and its chemical doping with foreign atoms (e.g., nitrogen),[5−10] there now exists an unprecedented opportunity to investigate the distribution of dopants in two dimensions with atomic-scale spatial precision.

Recently, we showed that individual dopants in graphene can be visualized using scanning tunneling microscopy/spectroscopy (STM/STS),[11,12] which provides both subatomic spatial resolution and compositional sensitivity through the measurement of electron tunneling characteristics at the surface.[13] In our previous studies, nitrogen-doped graphene was prepared on polycrystalline copper foil by chemical vapor deposition (CVD) from mixtures of methane and ammonia,[11] and because of the roughness of the copper-foil substrate, our initial attempts to study the distribution of dopants in these samples were limited to small scan areas, typically 30 nm × 30 nm. Nevertheless, our previous STM measurements revealed an unusual sublattice segregation of nitrogen dopants; of the two graphene sublattices, nitrogen dopants were found to predominantly occupy only one sublattice.[11,12] However, in certain other studies of nitrogen-doped graphene,[14,15] the sublattice segregation is not clearly observed. There are thus several open questions about dopant sublattice segregation, including the conditions under which it can be observed, the length scale of the segregated domains, and a microscopic understanding of the mechanism that drives the observed effect.

Here, in order to answer these questions, we have modified the graphene growth method by using single-crystal Cu(111) substrates, which allowed us to achieve large, atomically flat terraces of as-grown graphene, thus enabling investigations of dopant distributions on a large scale while maintaining atomic spatial resolution. Using these substrates, we have performed a systematic set of measurements to probe the influence of various sample-preparation conditions on the dopant sublattice distribution, and used density functional theory (DFT) to gain insight into the segregation process.

Our present STM measurements reveal large (up to 100 nm in size) well-separated domains where nitrogen dopants are located on the same sublattice. These sublattice domains are only present in samples grown by CVD, whereas other methods of nitrogen doping—such as reaction with ammonia or nitrogen ion bombardment—yield random distributions of sublattices. On the basis of DFT calculations, we attribute the observed segregation of sublattice domains in the CVD samples to the way in which the nitrogen atoms are incorporated into the graphene lattice during the growth process. Our findings,

Received: August 27, 2013
Published: January 6, 2014

   dx.doi.org/10.1021/ja408463g | J. Am. Chem. Soc. 2014, 136, 1391−1397

thus, provide new insights into the mechanism of graphene growth. Furthermore, the presence of doped sublattice domains could have important implications for extending the electronic applications of graphene through, for instance, band gap engineering.

RESULTS AND DISCUSSION

Preparation of Cu(111) with large atomic terraces was performed in an ultrahigh vacuum (UHV). The conventional CVD scheme for growing graphene was modified to take into account the UHV conditions,[16] in particular by replacing the precursor mixture of methane and ammonia with pyridine (C_5H_5N) as a single source of carbon and nitrogen.[17,18] The use of a large precursor molecule also allowed us to lower the precursor pressure to ~1 mTorr (compared to ~1 Torr for the conventional CVD growth), which is more compatible with the UHV environment.

Figure 1a shows an atomically resolved STM image of a CVD-grown nitrogen-doped sample. As reported previously,[11,14,15,19] the graphitic nitrogen dopants appear dark in STM images, whereas the carbon atoms adjacent to nitrogen appear bright due to an increase in the local density of states (DOS).

The unit cell of graphene consists of two carbon atoms, each occupying one of the two sublattices (*A* or *B*) that together constitute the honeycomb lattice of graphene. These sites are equivalent by symmetry in pristine graphene.[20] However, when carbon atoms are substituted by dopants, these two sublattices can behave differently. Simulated STM images, Figure 1b, show that charge transfer from nitrogen to graphene is maximized for carbon atoms that are located on the sublattice opposite to that containing nitrogen. These carbon atoms together form a triangle encompassing the bright region surrounding the nitrogen. Depending on the original sublattice position of the dopant, these triangular features appear as mirror images of each other, as illustrated by red and blue triangles in Figure 1b. This behavior thus allows us to resolve the sublattice position of each dopant in STM images; examples are highlighted in Figure 1a.

Figure 1c shows the STM topography of a larger area (20 nm × 20 nm) on a CVD-grown sample. Two important observations are noteworthy: First, the concentration of nitrogen dopants in the sample is 0.18%, which is much smaller than the original content of nitrogen in the precursor pyridine, 17%, indicating that the growth does not occur molecule by molecule; rather, the precursor breaks down into small fragments containing C or N. The growth of graphene then involves diffusion of these fragments on the surface until they reach a growing seed. The smaller content of nitrogen in graphene than in the precursor suggests that nitrogen, compared to carbon, either diffuses more slowly on the Cu(111) surface or reacts at a lower rate with graphene (the difference is ~100-fold in this case), or nitrogen has a shorter lifetime at the surface due to competing pathways such as migration into the copper substrate or desorption via formation of N_2. We note that the dopant concentration in the pyridine-grown samples is comparable to that in ammonia/methane grown samples,[11] indicating that similar growth mechanisms are operating in both cases.

The second striking observation is that all nitrogen dopants in Figure 1c are located on the same sublattice. This behavior clearly contradicts the natural expectation of random dopant

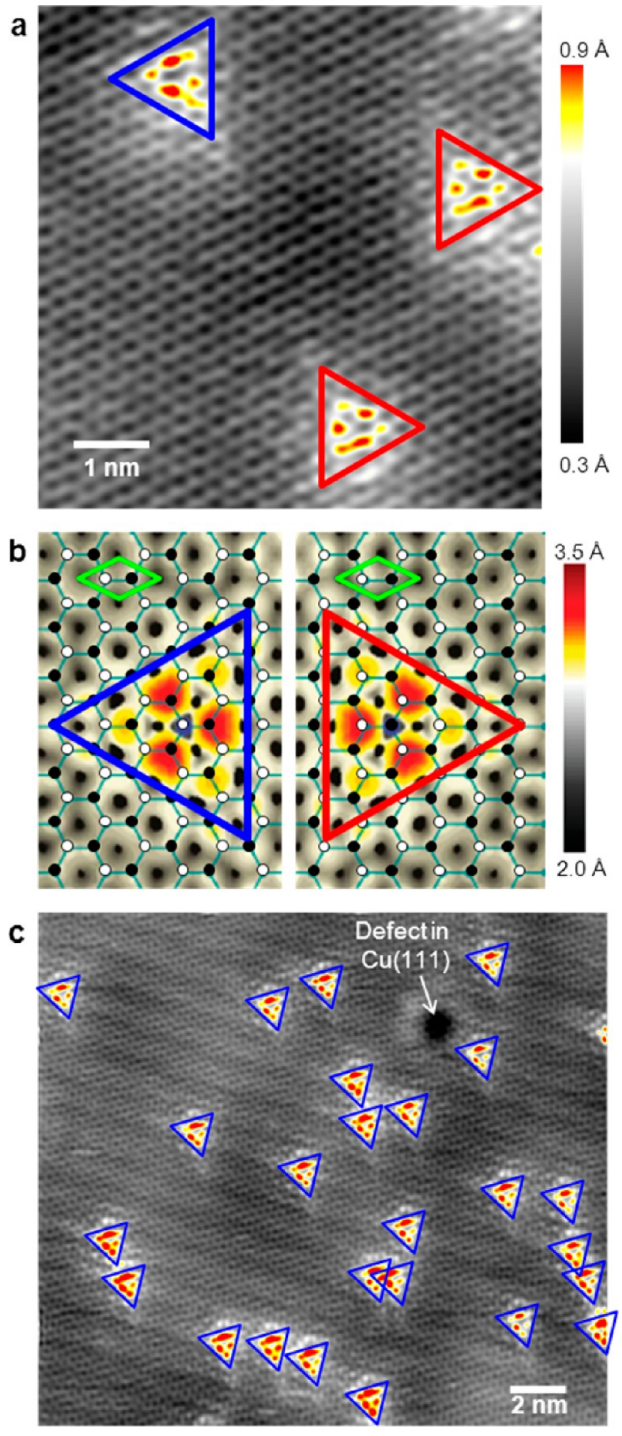

Figure 1. STM images of nitrogen-doped graphene. (a) STM image (7 × 7 nm^2, 1 V, 1 nA) of nitrogen-doped graphene on Cu(111) showing three dopants on two different sublattices. Bright colors in the STM image (red and yellow) correspond to carbon atoms surrounding nitrogen dopants, and red and blue triangles indicate dopants on different sublattices. (b) Simulated STM images of graphitic nitrogen dopants located on two different sublattices. Green diamonds indicate the unit cell of graphene, and black and white circles indicate the sublattices. Carbon atoms in the vicinity of the nitrogen dopants appear bright (red and yellow), forming triangles that appear as mirror images for the two sublattices (highlighted by red and blue triangles). (c) STM image (20 × 20 nm^2, 1 V, 1 nA) of CVD(pyridine)-grown nitrogen-doped graphene, showing all dopants located on the same sublattice.

dx.doi.org/10.1021/ja408463g | J. Am. Chem. Soc. 2014, 136, 1391−1397

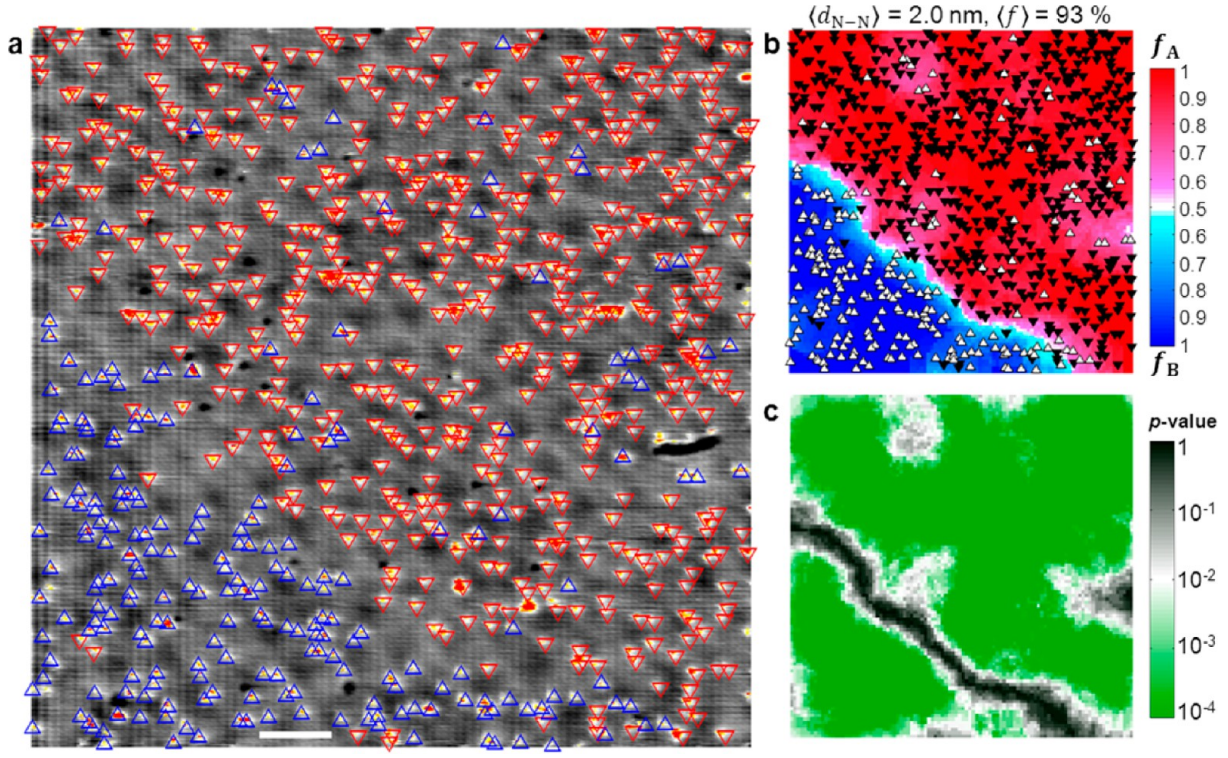

Figure 2. Distribution of nitrogen dopants in CVD(pyridine)-grown doped graphene. (a) STM image (100 × 100 nm^2, 1 V, 1 nA) of CVD-grown doped graphene on Cu(111). Dopant sublattices are highlighted by red (A) and blue (B) triangles. Scale bar = 10 nm. (b) Spatial analysis of sublattice distribution. ▼ = sublattice A. △ = sublattice B. f_A (or f_B) represents the fraction of dopants in sublattice A (or B) within a local radius. The color scale represents f_A and f_B and ranges from 0.5 (white) to 1 (red and blue for A and B, respectively). ⟨d_{N-N}⟩ = average interdopant separation. ⟨f⟩ = average degree of sublattice segregation. (c) Map of p-values corresponding to the ratios shown in map b, obtained under a null hypothesis.

distributions arising from equal probabilities of substituting the equivalent sublattices of graphene with nitrogen.

To further explore the distribution of dopant sublattices, we studied relatively large areas (100 nm × 100 nm) of graphene with atomic resolution. Figure 2a shows an example. We identified the sublattice position of each dopant as described above for Figure 1, and obtained the local distribution of dopants between sublattices A and B. This was done by calculating the ratio of the number of dopants in either sublattice (N_i; i = A, B) to the total number of dopants ($f_i = N_i/(N_A + N_B)$) within a local radius. To ensure statistical significance, a local radius of 5 times the average dopant separation (d_{N-N}) was used, corresponding to a sample size of $N \sim 25$. The resulting map is displayed in Figure 2b, where red or blue represent regions where either sublattice is dominant. The map clearly shows two well-separated red and blue domains, with an average degree of sublattice segregation of ⟨f⟩ = 93%.

To compare the observed sublattice segregation with a random distribution of dopants, we used a *null* hypothesis under which the dopants randomly occupy the two sublattices with an equal probability of P = 0.5. Such a random distribution would yield an expected value of P and a standard deviation of $(P(1 - P)/N)^{1/2}$. A comparison between the experimentally observed ratio, f, and the random distribution then would yield a p-value with which the likelihood of the null hypothesis can be evaluated. The corresponding map of p-values for this sample is shown in Figure 2c. A threshold of 0.01 is used (represented by white in the color scale), and for p-values less than the threshold (green regions), the null hypothesis can be rejected with a confidence level greater than 99%. These green domains clearly constitute the dominant portions of the map.

Interestingly, the size of the domains extends over 100 nm, and also there is a sharp boundary between the domains with a width of ∼1 nm, smaller than the average interdopant separation, ⟨d_{N-N}⟩ = 2 nm. Note that the boundary between the sublattice domains is independent of the structural grain boundaries in graphene. The image in Figure 2a involves a single lattice orientation of graphene, as evidenced by the observation of a uniform Moiré pattern[21] in the background. Further examples of sublattice domains in the CVD samples are shown in the Supporting Information, Figure S1, demonstrating the generality of this observation.

To investigate the cause of sublattice segregation, we examined a number of different methods for producing nitrogen-doped graphene. These included postsynthesis treatment of pristine graphene, by (a) reaction with ammonia or (b) nitrogen ion bombardment.[22,23] Figure 3 shows maps of dopant distributions resulting from these two methods, and they exhibit essentially a random distribution of sublattices, as evidenced by small degrees of segregation, ⟨f⟩ < 60%, and absence of continuous domains of p-values <0.01. This random distribution is in strong contrast to the observation of large sublattice domains in the CVD-grown samples.

Since the average dopant separation in samples prepared by different techniques was variable, we have analyzed the sublattice segregation, f, as a function of d_{N-N}, and the result is plotted in Figure 4. CVD samples exhibit large segregation ranging from ∼80 to 100%, mostly centered around the 85−95% range, whereas the post-treated samples exhibit

dx.doi.org/10.1021/ja408463g | J. Am. Chem. Soc. 2014, 136, 1391−1397

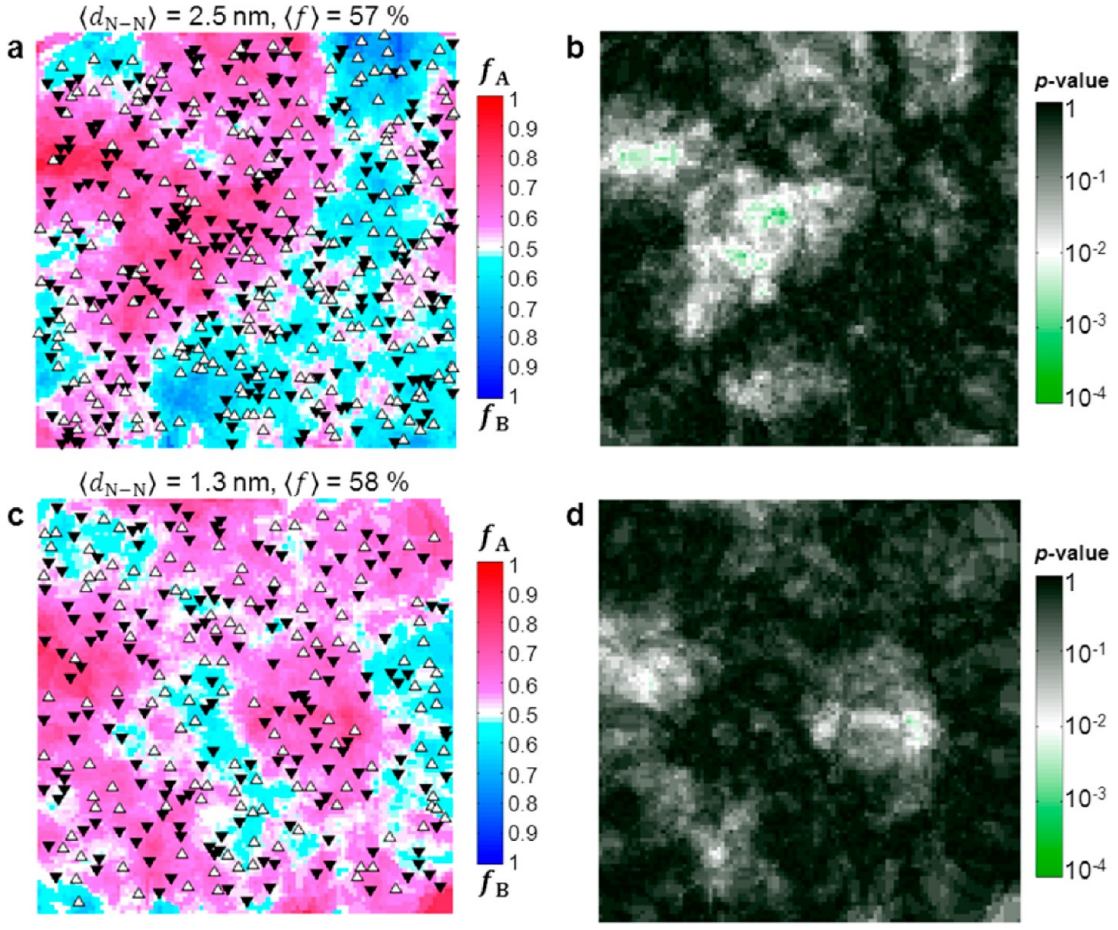

Figure 3. Spatial analysis of dopant distribution in postsynthesis doped graphene. (a, b) Graphene doped by reaction with ammonia. Map size 100 × 100 nm^2. (c, d) Graphene doped by nitrogen-ion bombardment. Map size 40 × 40 nm^2. (a, c) Local distribution of dopant sublattices and (b, d) the corresponding p-values.

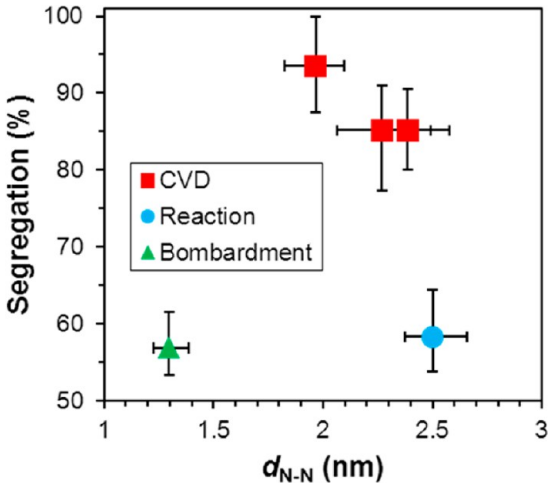

Figure 4. Sublattice segregation vs interdopant separation measured for five different samples prepared under various conditions: ■, CVD growth; ●, reaction with ammonia; ▲, nitrogen-ion bombardment. Error bars represent the interquartile range.

segregation approaching 50%. However, no systematic trend with d_{N-N} is observed among all the samples.

We rule out the electronic nature of interaction between nitrogen dopants as a driving force for the formation of sublattice domains in our samples. Theoretical calculations (see the Supporting Information, Figure S2, as well as refs 24 and 25) show that the N−N interaction in graphene is repulsive, relatively weak, and short-range, vanishing at less than 1 nm distance from the dopant site. However, experimentally, samples with large degrees of sublattice segregation (i.e., the CVD samples) exhibit ⟨d_{N-N}⟩ ∼ 2−3 nm, much longer than the operating range of the N−N interaction in graphene. Moreover, the ion-bombarded sample that has a small ⟨d_{N-N}⟩ of ∼1 nm, shows the least amount of sublattice segregation.

The fact that sublattice segregation is only observed in CVD samples suggests that sublattice selectivity is a consequence of the CVD growth. To shed light on the details of the growth process, we studied the energetics of nitrogen-doped graphene by performing DFT calculations for graphene nanoribbons on Cu(111). Two types of edges in the nanoribbon were considered: zigzag and Klein edges.[26,27] Our calculations show that, independent of the position of nitrogen, the graphene ribbon bends toward the substrate,[28−30] so that the terminating edge-atoms can form direct bonds with copper, as illustrated in Figure 5a. This achieves low-energy edge structures for the two distinct zigzag registries with the nearly lattice-matched Cu(111) substrate, with the terminal carbon atoms from each edge being from the same sublattice. However, this configuration results in significantly different energies for various substitutional positions of nitrogen, as presented in Figure 5b. We find that, in all cases, the energy is lower when nitrogen is located at the edge rather than inside

dx.doi.org/10.1021/ja408463g | J. Am. Chem. Soc. 2014, 136, 1391−1397

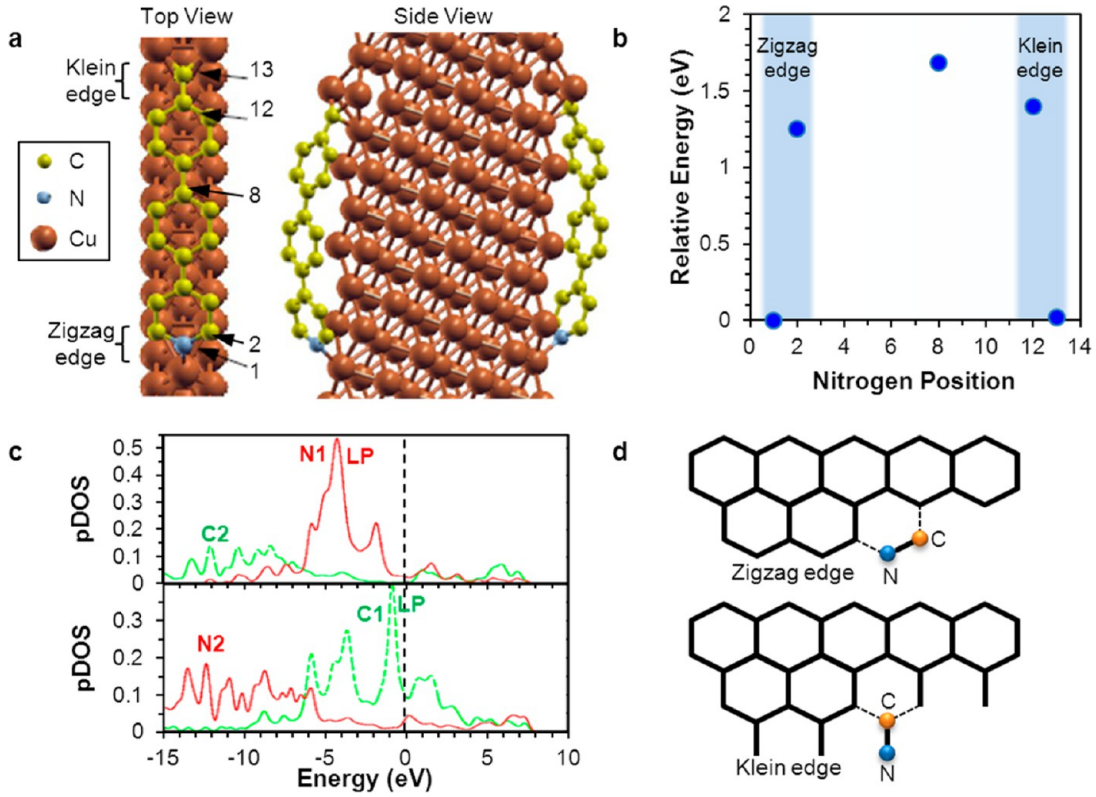

Figure 5. Calculated structure of nitrogen-doped graphene on Cu(111). (a) Optimized structure of a graphene nanoribbon, doped with nitrogen at one edge, on a Cu(111) slab. Two types of edges are included: zigzag (bottom edge, atoms 1 and 2) and Klein (top edge, atoms 12 and 13). (b) Relative energy of nitrogen-doped nanoribbon vs dopant position. Position 1 is chosen as the reference. (c) pDOS of the nanoribbon for the zigzag edge (atoms 1 and 2). Red curves respresent nitrogen, and green curves represent carbon. LP indicates the lone-pair state. (d) Schematics of a step-flow model for the CVD growth of graphene.

the ribbon,[31] while the zigzag edge is slightly more stable (<0.04 eV) than the Klein edge. More importantly, for either edge, the energy is lower by ∼1.3 eV when nitrogen is located on the outermost edge-atom (positions 1 vs 2 or 13 vs 12).[31] This energy gain is due to the formation of a nitrogen lone-pair at the graphene edge.[32] Figure 5c shows the lone-pair states at the zigzag edge of the nanoribbon for two cases: nitrogen located at position 1 or position 2. When nitrogen is at the edge (N1 in Figure 5c), the lone-pair state is lower in energy by ∼3 eV compared to the case where carbon is at the edge (C1 in Figure 5c), resulting in a higher affinity of nitrogen toward the graphene edge.

Recent theoretical studies of graphene growth on copper have reported that carbon dimers are the dominant growth intermediates, as they are more stable than adsorbed monomers by ∼2 eV.[33,34] When considering the addition of these intermediates to the growing edge of graphene in a step-flow picture (Figure 5d),[35−37] our calculations suggest that the dimers attach to the honeycomb lattice with a preferential orientation such that nitrogen is located at the outermost site. Given the energy difference of 1.3 eV between the two edge-sites, each corresponding to one sublattice of graphene, and the growth temperature of 950 °C, the equilibrium ratio between the numbers of nitrogen dopants in each sublattice would be a small fraction, 5×10^{-6}. As a result, of the two sublattices at the edge, one is preferred. As long as the relative atomic configuration between graphene and copper is preserved during growth, the step-flow picture replicates the same sublattice for nitrogen dopants row after row (Figure 5d), thus forming domains with preferential sublattices as observed experimentally.[38] However, we note that the experimental values of sublattice segregation are typically much smaller than the theoretical value estimated from the Boltzmann distribution, indicating that kinetic factors also play a role.

The observation of surprisingly large domain sizes (∼100 nm), substantially greater than intrinsic length scales in the graphene−copper system such as the Moiré pattern (max. 6 nm), points to structural details of the growth process. One scenario could be that individual islands of growing graphene, each dominated by one type of dopant sublattices, would merge and form sublattice domains with sharp boundaries. However, such a scenario would likely involve the formation of structural grain boundaries between the sublattice domains,[39,40] unless the islands are grown in perfect registry with the substrate. An alternative scenario is that the sharp transition between sublattice domains is caused by an abrupt change in the underlying Cu structure rather than the graphene itself. For instance, transient terrace steps or surface adatoms are readily formed at the fluidic surface of Cu at ∼1000 °C due to high surface mobility,[41] and graphene is known to grow continuously over various terraces and facets of the Cu substrate,[42] and induce surface reconstruction[43] such as step bunching[44] or terrace expansion.[45] It remains an open challenge for future modeling of graphene growth on Cu to understand the subtle interplay between Cu interface structure, the edge of the graphene lattice, and the adsorbed species that feed the growth, all at a growth temperature very close to the bulk Cu melting point (1085 °C).[46]

dx.doi.org/10.1021/ja408463g | J. Am. Chem. Soc. 2014, 136, 1391−1397

The ordered domains of dopant sublattices could have important implications. For example, in magnetic applications of graphene and spintronics, the unpaired electrons of the dopants can exhibit paramagnetic properties,[31,47,48] and the breaking of the sublattice symmetry can induce spin-polarized transport.[49,50] Moreover, a recent theoretical study of single-sublattice nitrogen-doped graphene[51] has shown that the unbalanced population of dopant sublattices results in the opening of a band gap in the graphene electronic structure, and the gap is tunable with dopant concentration; for example, 45 and 550 meV for 0.5 and 8% doping, respectively. The presence of such a band gap and the quasi-ballistic nature of carrier mobility in the unperturbed sublattice[51] offer new possibilities for graphene-based field-effect transistors.[52] Our efforts to measure charge transport in these sublattice-polarized materials are ongoing.

CONCLUSION

In summary, nitrogen dopants in CVD(pyridine)-grown graphene prefer to occupy the same sublattices, forming well-separated domains as large as 100 nm. These sublattice domains are formed only when dopants are incorporated into graphene during growth; they are absent when pristine graphene is doped postsynthesis by reaction with ammonia or by nitrogen ion bombardment. The observation of sublattice segregation in CVD(pyridine)-grown samples, therefore, provides important information about the mechanism of graphene growth on copper—a popular approach for large-scale production of graphene—and opens up new possibilities to tailor the properties of graphene for electronic and magnetic applications.

METHODS

Experiment. The Cu(111) substrate was prepared in a UHV chamber (base pressure 2.0×10^{-10} Torr) by repeated cycles of argon-ion sputtering (2 kV, 1.1×10^{-5} Torr, 15 min) and annealing (650 °C, 20 min). For CVD growth, the substrate was heated in the UHV chamber at 950 °C and pyridine (Sigma-Aldrich, anhydrous, 99.8%) was background dosed at 0.5−1 mTorr for 5−10 min. The sample was then further annealed at 950 °C for 20−30 min. Pyridine was introduced to the UHV system following several cycles of freeze−pump−thaw.

Reaction of graphene with ammonia was carried out in the UHV chamber by heating a pristine graphene sample on copper at 950 °C and dosing ammonia (Matheson, 99%) at 1 mTorr for 30 min. The sample was annealed additionally for 30 min. A detailed study of the reaction will be published elsewhere.

Bombardment of graphene with nitrogen ions was also performed in the UHV chamber. Nitrogen gas (Tech Air, ultrahigh purity) was bombarded at 100 V and 5×10^{-6} Torr onto pristine graphene on copper at room temperature.[23] The sample was subsequently annealed at 950 °C for 30 min to heal the defects created by the ion bombardment.

STM measurements were performed using an Omicron VT-STM operating under UHV and at room temperature. STM tips were prepared by electrochemical etching of tungsten wires in a 3 M NaOH solution, and were cleaned in UHV by annealing at 800 °C for 30 min. Images were obtained in the constant-current mode.

Theory. First-principles calculations were performed using DFT within the local density approximation (LDA) as implemented in the Quantum Espresso (QE) package.[53] Norm-conserving pseudopotentials with Perdew−Zunger (NC-PZ) fit of the Ceperley−Alder electron gas results for exchange and correlation provided with the package (Von Barth−Car direct fit) were used for STM simulations with four valence electrons for carbon and five valence electrons for nitrogen and an energy cutoff of 95 Ry for the plane-wave basis set. The STM image simulation was carried out using the Tersoff−Hamann approach,[54] on a 7 × 7 nitrogen-doped graphene supercell including 98 atoms. We applied a bias voltage of +0.5 V, hence probing the empty states of nitrogen-doped graphene.

To calculate pDOS on individual atoms, a 12 × 12 nitrogen-doped graphene supercell with 288 atoms was used. This relatively large supercell gives a N−N separation of 3 nm which is comparable to the experimental average value of 2−3 nm present in our samples. We modeled the N-doped graphene by substituting one carbon in the monolayer graphene by nitrogen and performing structural relaxation of the resulting structure until the forces were less than 10^{-3} Ry/au. We used Vanderbilt ultrasoft pseudopotentials with the PBE exchange-correlation functional as implemented in the QE package, with the lattice constant 1.43 Å (compared to the NC-PZ lattice constant of 1.41 Å). Nitrogen remained coplanar with the surrounding graphene, with a nearest neighbor N−C distance of 1.42 Å (compared to 1.40 Å for NC-PZ).

The graphene ribbon was constructed using 13 atoms and two different Klein and zigzag edges, with or without a copper substrate. The Cu(111) substrate was modeled with seven copper layers and was strained with the lattice constant of pristine graphene, 2.44 Å. We used ultrasoft pseudopotentials (A. Dal Corso) with the PZ exchange-correlation functional as implemented in the QE package with 11, 5, and 4 valence electrons for Cu, N, and C, respectively. The energy cutoff was 25 Ry, and a uniform (12 × 1 × 1) Monkhorst−Pack *k*-point grid was used. Substitutional nitrogen was introduced into the graphene ribbon at different sites, and structural relaxation was performed until the forces were less than 10^{-3} Ry/au. In view of the substantial distortion observed in Figure 5a, we also considered the role of van der Waals interactions using the semiempirical approach of Grimme.[55] The center of the ribbon is indeed pulled closer to the Cu surface in this case, but the relative energy for N substitution in the different sites remains the same as reported in Figure 5b within 0.1 eV. The effect, therefore, is dominated by specific chemical interactions between Cu and C versus N.

ASSOCIATED CONTENT

Supporting Information

(S1) STM images and maps of dopant distribution for additional CVD-grown samples. (S2) Calculated electronic structure of nitrogen-doped graphene. This material is available free of charge via the Internet at http://pubs.acs.org.

AUTHOR INFORMATION

Corresponding Author

gwf1@columbia.edu

Notes

The authors declare no competing financial interest.

ACKNOWLEDGMENTS

This work was funded by the Department of Energy under Grant Nos. DE-FG02-88ER13937 (G.W.F.), EFRC Award DE-SC0001085 (G.W.F., A.N.P., D.R.R.) and for work done in part at the Center for Functional Nanomaterials, Brookhaven National Laboratory, under Contract No. DE-AC02-98CH10886, and by the Air Force Office of Scientific Research (MURI FA955009-1-0705). We acknowledge financial support from the New York State Office of Science, Technology, and Academic Research (NYSTAR). Equipment support was provided by the National Science Foundation under grant CHE-10-12058 (G.W.F.). A.N.P. also acknowledges salary support provided by Defense Advanced Research Projects Agency grant no. N66001-12-1-4216 and Air Force Office for Scientific Research under grant no. FA9550-11-1-0010.

REFERENCES

(1) Sze, S. M. *Physics of semiconductor devices*, 2nd ed.; Wiley: New York, 1981; p 16−27.
(2) Norris, D. J.; Efros, A. L.; Erwin, S. C. *Science* **2008**, *319*, 1776−1779.
(3) McElroy, K.; Lee, J.; Slezak, J. A.; Lee, D. H.; Eisaki, H.; Uchida, S.; Davis, J. C. *Science* **2005**, *309*, 1048−1052.
(4) Shinada, T.; Okamoto, S.; Kobayashi, T.; Ohdomari, I. *Nature* **2005**, *437*, 1128−1131.
(5) Panchakarla, L. S.; Govindaraj, A.; Rao, C. N. R. *Inorg. Chim. Acta* **2010**, *363*, 4163−4174.
(6) Georgakilas, V.; Otyepka, M.; Bourlinos, A. B.; Chandra, V.; Kim, N.; Kemp, K. C.; Hobza, P.; Zboril, R.; Kim, K. S. *Chem. Rev.* **2012**, *112*, 6156−6214.
(7) Batzill, M. *Surf. Sci. Rep.* **2012**, *67*, 83−115.
(8) Liu, H. T.; Liu, Y. Q.; Zhu, D. B. *J. Mater. Chem.* **2011**, *21*, 3335−3345.
(9) Wang, H. T.; Wang, Q. X.; Cheng, Y. C.; Li, K.; Yao, Y. B.; Zhang, Q.; Dong, C. Z.; Wang, P.; Schwingenschlogl, U.; Yang, W.; Zhang, X. X. *Nano Lett.* **2012**, *12*, 141−144.
(10) Wang, H. B.; Maiyalagan, T.; Wang, X. *ACS Catal.* **2012**, *2*, 781−794.
(11) Zhao, L.; He, R.; Rim, K. T.; Schiros, T.; Kim, K. S.; Zhou, H.; Gutierrez, C.; Chockalingam, S. P.; Arguello, C. J.; Palova, L.; Nordlund, D.; Hybertsen, M. S.; Reichman, D. R.; Heinz, T. F.; Kim, P.; Pinczuk, A.; Flynn, G. W.; Pasupathy, A. N. *Science* **2011**, *333*, 999−1003.
(12) Zhao, L.; Levendorf, M.; Goncher, S.; Schiros, T.; Palova, L.; Zabet-Khosousi, A.; Rim, K. T.; Gutierrez, C.; Nordlund, D.; Jaye, C.; Hybertsen, M.; Reichman, D.; Flynn, G. W.; Park, J.; Pasupathy, A. N. *Nano Lett.* **2013**, *13*, 4659−65.
(13) Andrei, E. Y.; Li, G. H.; Du, X. *Rep. Prog. Phys.* **2012**, *75*, 056501.
(14) Joucken, F.; Tison, Y.; Lagoute, J.; Dumont, J.; Cabosart, D.; Zheng, B.; Repain, V.; Chacon, C.; Girard, Y.; Botello-Mendez, A. R.; Rousset, S.; Sporken, R.; Charlier, J. C.; Henrard, L. *Phys. Rev. B* **2012**, *85*, 161408(R).
(15) Lv, R.; Li, Q.; Botello-Mendez, A. R.; Hayashi, T.; Wang, B.; Berkdemir, A.; Hao, Q. Z.; Elias, A. L.; Cruz-Silva, R.; Gutierrez, H. R.; Kim, Y. A.; Muramatsu, H.; Zhu, J.; Endo, M.; Terrones, H.; Charlier, J. C.; Pan, M. H.; Terrones, M. *Sci. Rep.* **2012**, *2*, 586.
(16) Zhao, L.; Rim, K. T.; Zhou, H.; He, R.; Heinz, T. F.; Pinczuk, A.; Flynn, G. W.; Pasupathy, A. N. *Solid State Commun.* **2011**, *151*, 509−513.
(17) Usachov, D.; Vilkov, O.; Gruneis, A.; Haberer, D.; Fedorov, A.; Adamchuk, V. K.; Preobrajenski, A. B.; Dudin, P.; Barinov, A.; Oehzelt, M.; Laubschat, C.; Vyalikh, D. V. *Nano Lett.* **2011**, *11*, 5401−5407.
(18) Jin, Z.; Yao, J.; Kittrell, C.; Tour, J. M. *ACS Nano* **2011**, *5*, 4112−4117.
(19) Zheng, B.; Hermet, P.; Henrard, L. *ACS Nano* **2010**, *4*, 4165−4173.
(20) Cheianov, V. V.; Syljuasen, O.; Altshuler, B. L.; Fal'ko, V. I. *Europhys. Lett.* **2010**, *89*, 56003.
(21) Gao, L.; Guest, J. R.; Guisinger, N. P. *Nano Lett.* **2010**, *10*, 3512−3516.
(22) Kim, K. J.; Yang, S.; Park, Y.; Lee, M.; Kim, B.; Lee, H. *J. Phys. Chem. C* **2013**, *117*, 2129−2134.
(23) Zhao, W.; Hofert, O.; Gotterbarm, K.; Zhu, J. F.; Papp, C.; Steinruck, H. P. *J. Phys. Chem. C* **2012**, *116*, 5062−5066.
(24) Lambin, P.; Amara, H.; Ducastelle, F.; Henrard, L. *Phys. Rev. B* **2012**, *86*, 045448.
(25) Xiang, H. J.; Huang, B.; Li, Z. Y.; Wei, S. H.; Yang, J. L.; Gong, X. G. *Phys. Rev. X* **2012**, *2*, 011003.
(26) Klein, D. J. *Chem. Phys. Lett.* **1994**, *217*, 261−265.
(27) Suenaga, K.; Koshino, M. *Nature* **2010**, *468*, 1088−1090.
(28) Lacovig, P.; Pozzo, M.; Alfe, D.; Vilmercati, P.; Baraldi, A.; Lizzit, S. *Phys. Rev. Lett.* **2009**, *103*, 166101.
(29) Gao, J. F.; Yip, J.; Zhao, J. J.; Yakobson, B. I.; Ding, F. *J. Am. Chem. Soc.* **2011**, *133*, 5009−5015.
(30) Van Wesep, R. G.; Chen, H.; Zhu, W. G.; Zhang, Z. Y. *J. Chem. Phys.* **2011**, *134*, 171105.
(31) Cruz-Silva, E.; Barnett, Z. M.; Sumpter, B. G.; Meunier, V. *Phys. Rev. B* **2011**, *83*, 155445.
(32) Schiros, T.; Nordlund, D.; Palova, L.; Prezzi, D.; Zhao, L.; Kim, K. S.; Wurstbauer, U.; Gutierrez, C.; Delongchamp, D.; Jaye, C.; Fischer, D.; Ogasawara, H.; Pettersson, L. G. M.; Reichman, D. R.; Kim, P.; Hybertsen, M. S.; Pasupathy, A. N. *Nano Lett.* **2012**, *12*, 4025−4031.
(33) Chen, H.; Zhu, W. G.; Zhang, Z. Y. *Phys. Rev. Lett.* **2010**, *104*, 186101.
(34) Riikonen, S.; Krasheninnikov, A. V.; Halonen, L.; Nieminen, R. M. *J. Phys. Chem. C* **2012**, *116*, 5802−5809.
(35) Artyukhov, V. I.; Liu, Y. Y.; Yakobson, B. I. *Proc. Natl. Acad. Sci. U.S.A.* **2012**, *109*, 15136−15140.
(36) Shu, H. B.; Chen, X. S.; Tao, X. M.; Ding, F. *ACS Nano* **2012**, *6*, 3243−3250.
(37) Luo, Z.; Kim, S.; Kawamoto, N.; Rappe, A. M.; Johnson, A. T. C. *ACS Nano* **2011**, *5*, 9154−60.
(38) We did not explicitly consider armchair edges or their variants here. The A5′ variant from ref 35 has a similar, one-fold, terminal C atom that can have low energy due to bonding with the Cu substrate. We expect N would preferentially occupy this site for the same reasons found for the Klein edge.
(39) Huang, P. Y.; Ruiz-Vargas, C. S.; van der Zande, A. M.; Whitney, W. S.; Levendorf, M. P.; Kevek, J. W.; Garg, S.; Alden, J. S.; Hustedt, C. J.; Zhu, Y.; Park, J.; McEuen, P. L.; Muller, D. A. *Nature* **2011**, *469*, 389−392.
(40) Kim, K.; Lee, Z.; Regan, W.; Kisielowski, C.; Crommie, M. F.; Zettl, A. *ACS Nano* **2011**, *5*, 2142−6.
(41) Brune, H. *Ann. Phys.* **2009**, *18*, 675−698.
(42) Rasool, H. I.; Song, E. B.; Allen, M. J.; Wassei, J. K.; Kaner, R. B.; Wang, K. L.; Weiller, B. H.; Gimzewski, J. K. *Nano Lett.* **2011**, *11*, 251−256.
(43) Tian, J.; Cao, H.; Wu, W.; Yu, Q.; Guisinger, N. P.; Chen, Y. P. *Nano Lett.* **2012**, *12*, 3893−3899.
(44) Hayashi, K.; Sato, S.; Yokoyama, N. *Nanotechnology* **2013**, *24*, 025603.
(45) Gunther, S.; Danhardt, S.; Wang, B.; Bocquet, M. L.; Schmitt, S.; Wintterlin, J. *Nano Lett.* **2011**, *11*, 1895−900.
(46) Zhang, W.; Wu, P.; Li, Z.; Yang, J. *J. Phys. Chem. C* **2011**, *115*, 17782−17787.
(47) Nair, R. R.; Sepioni, M.; Tsai, I. L.; Lehtinen, O.; Keinonen, J.; Krasheninnikov, A. V.; Thomson, T.; Geim, A. K.; Grigorieva, I. V. *Nat. Phys.* **2012**, *8*, 199−202.
(48) Rhim, S. H.; Qi, Y.; Liu, Y.; Weinert, M.; Li, L. *Appl. Phys. Lett.* **2012**, *100*, 233119.
(49) Park, H.; Wadehra, A.; Wilkins, J. W.; Neto, A. H. C. *Phys. Rev. B* **2013**, *87*, 085441.
(50) Soriano, D.; Fernandez-Rossier, J. *Phys. Rev. B* **2012**, *85*, 195433.
(51) Lherbier, A.; Botello-Mendez, A. R.; Charlier, J. C. *Nano Lett.* **2013**, *13*, 1446−1450.
(52) Schwierz, F. *Nat. Nanotechnol.* **2010**, *5*, 487−496.
(53) Giannozzi, P.; Baroni, S.; Bonini, N.; Calandra, M.; Car, R.; Cavazzoni, C.; Ceresoli, D.; Chiarotti, G. L.; Cococcioni, M.; Dabo, I.; Dal Corso, A.; de Gironcoli, S.; Fabris, S.; Fratesi, G.; Gebauer, R.; Gerstmann, U.; Gougoussis, C.; Kokalj, A.; Lazzeri, M.; Martin-Samos, L.; Marzari, N.; Mauri, F.; Mazzarello, R.; Paolini, S.; Pasquarello, A.; Paulatto, L.; Sbraccia, C.; Scandolo, S.; Sclauzero, G.; Seitsonen, A. P.; Smogunov, A.; Umari, P.; Wentzcovitch, R. M. *J. Phys.: Condens. Matter* **2009**, *21*, 395502.
(54) Tersoff, J.; Hamann, D. R. *Phys. Rev. B* **1985**, *31*, 805−813.
(55) Grimme, S. *J. Comput. Chem.* **2006**, *27*, 1787−1799.